Front. Chem. Sci. Eng. 2022, 16(11): 1616−1622
https://doi.org/10.1007/s11705-022-2183-x

RESEARCH ARTICLE

Efficient acetylene/carbon dioxide separation with excellent dynamic capacity and low regeneration energy by anion-pillared hybrid materials

Yijian Li[1], Jianbo Hu[2], Jiyu Cui[1], Qingju Wang[1], Huabin Xing[1,2], Xili Cui (✉)[1,2]

1 Zhejiang Key Laboratory of Smart Biomaterials, Key Laboratory of Biomass Chemical Engineering of Ministry of Education, College of Chemical and Biological Engineering, Zhejiang University, Hangzhou 310027, China
2 ZJU-Hangzhou Global Scientific and Technological Innovation Center, Hangzhou 311215, China

Abstract Adsorptive separation of acetylene/carbon dioxide mixtures by porous materials is an important and challenging task due to their similar sizes and physical properties. Here, remarkable acetylene/carbon dioxide separation featuring a high dynamic breakthrough capacity for acetylene (4.3 mmol·g^{-1}) as well as an ultralow acetylene regeneration energy (29.5 kJ·mol^{-1}) was achieved with the novel TiF_6^{2-}-pillared material ZU-100 (TIFSIX-bpy-Ni). Construction of a pore structure with abundant TiF_6^{2-} anion sites and pores with appropriate sizes enabled formation of acetylene clusters through hydrogen bonds and intermolecular interactions, which afforded a high acetylene capacity (8.3 mmol·g^{-1}) and high acetylene/carbon dioxide uptake ratio (1.9) at 298 K and 1 bar. Moreover, the NbO_5^{2-} anion-pillared material ZU-61 investigated for separation of acetylene/carbon dioxide. In addition, breakthrough experiments were also conducted to further confirm the excellent dynamic acetylene/carbon dioxide separation performance of ZU-100.

Keywords adsorption, acetylene/carbon dioxide separation, dynamic capacity, anion-pillared hybrid material

1 Introduction

Acetylene (C_2H_2) is one of the fundamental raw materials used for manufacturing various organic chemicals and is generally produced by partial combustion of natural gases or decomposition of calcium carbide. To obtain pure C_2H_2, CO_2 impurities must be removed. However, due to the similarities in physical properties (boiling points: C_2H_2, 198.3 K; CO_2, 194.7 K) and molecular sizes (C_2H_2, 3.3 Å × 3.3 Å × 5.7 Å; CO_2, 3.2 Å × 3.3 Å × 5.4 Å) [1], it is very difficult and challenging to separate these two molecules. In industry, C_2H_2/CO_2 separation currently depends primarily on bulk extraction by organic solvents or cryogenic distillation, which are costly and energy intensive. Physisorption with porous materials has been demonstrated to be an alternative enabling C_2H_2/CO_2 separation in an efficient and eco-friendly manner.

Metal organic frameworks (MOFs), also known as porous coordination polymers, are considered as some of the most promising physical adsorbents due to their diverse topologies and tunable structures [2–15]. Studies on the use of MOFs for C_2H_2/CO_2 separation are widely reported [16–25]. To achieve high C_2H_2/CO_2 separation selectivity, strong adsorption sites, such as amino groups [26], uncoordinated metal sites [27], and Cu^I ion sites [28], have been used to enhance binding of C_2H_2 over that of CO_2. However, strong binding leads required energy consumption for regeneration. Therefore, construction of porous materials with appropriate adsorption sites and suitable pore sizes is essential for C_2H_2/CO_2 separation. Electrostatic anion adsorption sites are selective and have been widely investigated. In previous studies, the SiF_6^{2-} anion pillared hybrid materials SIFSIX-3-Ni (3.8 Å) and SIFSIX-2-Cu-i (5.1 Å) have been investigated for separation of C_2H_2/CO_2 [29–32]. Interestingly, SIFSIX-3-Ni and SIFSIX-2-Cu-i showed opposite C_2H_2/CO_2 separation selectivities, which demonstrates that subtle tuning of the pore structures and geometries of binding sites has a great influence on separation performance. However, the C_2H_2 capacities of SIFSIX-3-Ni and SIFSIX-2-Cu-i are relatively modest due to their low surface areas and pore volumes. To further explore and promote C_2H_2/CO_2

Received March 27, 2022; accepted May 8, 2022

E-mail: cuixl@zju.edu.cn

separation by anion-pillared hybrid materials, we introduced anion adsorption sites into the target materials and precisely designed the pore sizes and geometries of binding sites. Finally, different pore structures were constructed by using the ligand 4,4'-bipyridine. Specifically, two anion-pillared hybrid materials, NbOFFIVE-bpy-Ni (NbOFFIVE = $NbOF_5^{2-}$, bpy = 4,4'-bipyridine, also termed ZU-61) and TIFSIX-bpy-Ni (TIFSIX = TiF_6^{2-}, also termed ZU-100), showed relatively large pore sizes of 7.8 Å. Adsorption experiments confirmed the increased C_2H_2 uptake capacities of ZU-61 (6.4 $mmol \cdot g^{-1}$) and ZU-100 (8.3 $mmol \cdot g^{-1}$) at 298 K and 1 bar. Moreover, the C_2H_2/CO_2 selectivity of ZU-100 (7.6) was higher than those of SIFSIX-3-Ni (0.13) and SIFSIX-2-Cu-i (6.5) [31]. Detailed analysis revealed that four C_2H_2 molecules were strongly adsorbed in every unit cell through C–H···F hydrogen bonds as well as multiple $H^{\delta+}\cdots C^{\delta-}$ dipole–dipole interactions between C_2H_2 molecules. However, CO_2 molecules only formed relatively weak van der Waals interactions with a single F atom due to expansion of the pore. Breakthrough experiments confirmed the excellent dynamic separation efficiency and improved dynamic capacity for C_2H_2 adsorption.

2 Experimental

Synthesis of $NiNbOF_5$. Firstly, 0.7471 g NiO, 1.33 g Nb_2O_5 and 4 mL HF were added into a PTFE reactor and stirred until fully dissolved, then the mixture was kept at 100 °C for 24 h. Take the supernatant into non-glass container and heated to 90 °C for evaporation crystallization. Then we got the $NiNbOF_5$. The infrared spectrum of $NiNbOF_5$ was shown at Fig. S1 (cf. Electronic Supplementary Material, ESM).

Synthesis of ZU-61 powder. An ethylene glycol solution (40 mL) of 4,4'-bipyridine (0.35 g) and an aqueous solution (20 mL) of $NiNbOF_5$ (0.41 g) were mixed and heated at 65 °C for 1 h under stirring. The obtained powder was filtered and washed with methanol.

Synthesis of ZU-100 powder. An ethylene glycol solution (40 mL) of 4,4'-bipyridine (0.35 g) and a methanol solution (20 mL) of $(NH_4)_2TiF_6$ (0.41 g) and $Ni(BF_4)_2$ (0.19 g) were mixed and heated at 65 °C overnight under stirring. The obtained powder was filtered and washed with methanol.

Synthesis of ZU-61 single crystal. The single crystals of ZU-61 were synthesized by slow diffusion of a methanol solution (4.0 mL) of $NiNbOF_5$ (0.03 g) into an ethylene glycol solution (4.0 mL) of 4,4'-bipyridine (0.03 g) after a week.

Characterization of ZU-100 and ZU-61. Powder X-ray diffraction (PXRD) and single crystal X-ray diffraction data were collected on a SHIMADZU XRD-6000 diffractometer and a Bruker APEX-II CCD diffractometer, respectively. Surface area was based on the nitrogen adsorption and desorption isotherms at 77 K using micromeritics ASAP 2460 adsorption apparatus. The thermal gravimetric analysis was performed on an instrument of TGA Q500 V20.13 Build 39. More details could be seen in ESM.

Gas adsorption measurements. C_2H_2 and CO_2 gas adsorption measurements were performed on the Micromeritics ASAP 2460. Before gas adsorption measurements, the sample of ZU-61 and ZU-100 were evacuated at 65 °C for 12 h until the pressure dropped below 1 Pa. The sorption isotherms were collected at 283–313 K on activated samples.

Column breakthrough experiments for C_2H_2/CO_2 gas mixture. The breakthrough experiments were accomplished by a dynamic gas breakthrough equipment. The experiment was conducted using a stainless-steel column (4.6 mm inner diameter × 50 mm). The weight of ZU-61 and ZU-100 powder packed in the column was 0.2816 and 0.2588 g. The column packed with sample was activated with N_2 flow (15 $mL \cdot min^{-1}$) for 12 h at 65 °C. After activation, the mixed gas (C_2H_2/CO_2=50/50, v/v) flow was introduced at 2 $mL \cdot min^{-1}$. Outlet gas from the column was monitored using gas chromatography (GC-490) with a thermal conductivity detector. After the breakthrough experiment, the sample was regenerated with N_2 flow (15 $mL \cdot min^{-1}$) for about 12 h at 65 °C. Detailed calculation methods for dynamic capacity and separation factors were shown in supplementary information and Fig. S2 (cf. ESM).

Dispersion-corrected density-functional theory (DFT) calculations. To further understand the interactions between guests and host framework, DFT method was utilized to calculate the binding energies of C_2H_2 and CO_2 molecules. More details could be seen in ESM.

3 Results and discussion

ZU-100 is a new material synthesized from 4,4'-bipyridine, TiF_6^{2-} and Ni^{2+} through a hydrothermal reaction. As shown in Fig. 1, two-dimensional (2D) nets of organic ligands (4,4'-bipyridine) and metal nodes (Ni^{2+}) were pillared with TiF_6^{2-} anions in the third dimension to form three-dimensional coordination networks with a pcu topology (Figs. 1(a) and 1(b)). The maximum F–F distance of the pore aperture in ZU-100 was 12.15 Å, while the minimum H–H distance was 9.91 Å (Fig. 1(c)), which is much larger than the pore sizes of SIFSIX-3-Ni (3.8 Å) and SIFSIX-2-Cu-i (5.1 Å) [31]. ZU-61 is isostructural with ZU-100 containing $NbOF_5^{2-}$ anions [33]. The TiF_6^{2-} anion is smaller than the $NbOF_5^{2-}$ anion, which led to a ZU-100 pore size larger than that of ZU-61 (F–F distance: 12.11 Å; H–H distance: 9.25 Å).

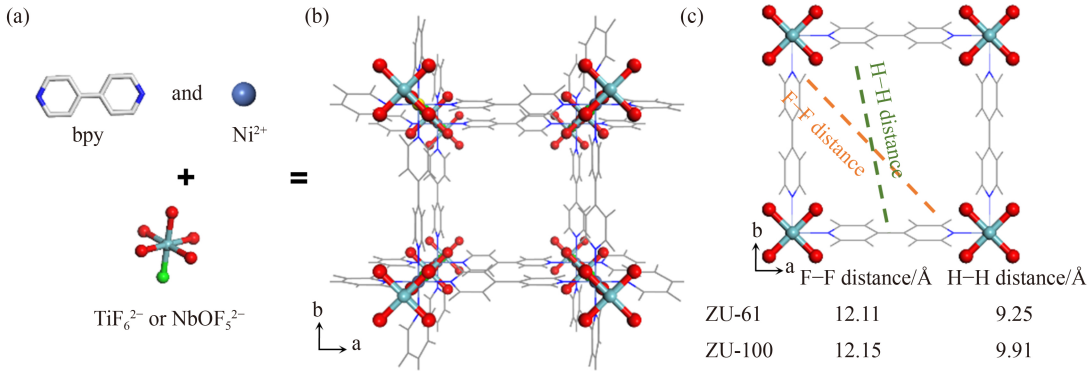

Fig. 1 Schematic representations of ZU-61 and ZU-100. (a) Sketch of metal node, inorganic pillar and ligand with the pyridine H atoms omitted for clarity; (b) the perspective view of the skeleton structure of ZU-61 and ZU-100; (c) the skeleton structure of ZU-61 and ZU-100 viewed along the c axis, the F–F and H–H distance of the two structures (Color code: F red; C and H gray; Ni purple; Nb and Ti cyan; O green; N blue).

The Ni–Ni distances between the two 2D nets of the two materials were also different, which were 7.931 and 7.836 Å for ZU-100 and ZU-61, respectively. Moreover, the stronger electrostatic potential of TiF_6^{2-} anions provided stronger adsorption sites for C_2H_2 molecules. The N_2 adsorption–desorption isotherms of ZU-61 and ZU-100 at 77 K were measured for further investigation, as depicted in Figs. S3 and S4 (cf. ESM). The Brunauer–Emmett–Teller (BET) surface areas were calculated to be 1022 and 1161 $m^2 \cdot g^{-1}$ for ZU-61 and ZU-100, respectively, much higher than the BET surface areas of SIFSIX-3-Ni (368 $m^2 \cdot g^{-1}$), SIFSIX-2-Cu-i (503 $m^2 \cdot g^{-1}$) [31] and benchmark materials UTSA-300 [35] (311 $m^2 \cdot g^{-1}$) and CPL-1-NH_2 [26] (103 $m^2 \cdot g^{-1}$), which indicated the potential for high C_2H_2 capacity. Relevant stability analyses, including thermogravimetric analysis (Fig. S5, cf. ESM) and water stability analysis (Fig. S6, cf. ESM), were undertaken. The thermogravimetric curve of ZU-100 showed that ZU-100 underwent no significant loss of quality until 250 °C, which is lower than the decomposition temperature of ZU-61 (320 °C) [33]. PXRD data demonstrated the integrity of the crystal structure of ZU-100 after exposure to wet air for one day.

The single-component adsorption isotherms of C_2H_2 and CO_2 on ZU-61 and ZU-100 were collected to further investigate the adsorption properties. As depicted in Fig. 2, the C_2H_2 isotherms for adsorption on ZU-61 and ZU-100 at 298 K both exhibited type-I microporous adsorption behavior (Fig. 2(a)). The saturated C_2H_2 uptake of ZU-100 at 1 bar and 298 K was 8.3 $mmol \cdot g^{-1}$, while ZU-61 showed a lower C_2H_2 uptake of 6.4 $mmol \cdot g^{-1}$ under the same conditions; these values were higher than those of SIFSIX-3-Ni (3.3 $mmol \cdot g^{-1}$) [30], SIFSIX-2-Cu-i (4.1 $mmol \cdot g^{-1}$) [31] and other benchmark materials, such as UTSA-300 (3.1 $mmol \cdot g^{-1}$) [34], CPL-1-NH_2 (1.8 $mmol \cdot g^{-1}$) [27] and JCM-1 (3.4 $mmol \cdot g^{-1}$) [35]. Both materials exhibited strong affinity for C_2H_2, which was demonstrated by high C_2H_2 uptake levels at low pressures. The C_2H_2 uptake capacities on ZU-61 and ZU-100 at 0.1 bar and 298 K were 3.0 and 2.3 $mmol \cdot g^{-1}$, respectively. The difference in C_2H_2 capacities between the two materials was mainly attributed to the larger BET area and lower cell density of ZU-100 (0.88 $cm^3 \cdot g^{-1}$) relative to ZU-61 (0.95 $cm^3 \cdot g^{-1}$). The CO_2 adsorption affinities of the two materials were much weaker than the C_2H_2 affinities. The CO_2 uptake levels increased slowly with increasing pressure and reached 4.4 and 2.7 $mmol \cdot g^{-1}$ for ZU-100 and ZU-61 at 1 bar and 298 K, respectively. The C_2H_2/CO_2 uptake ratios at 1 bar were calculated to compare the C_2H_2/CO_2 selectivities of different materials. The C_2H_2/CO_2 uptake ratios for ZU-61 and ZU-100 at 1 bar were 2.3 and 1.9, which were higher than those of SIFSIX-3-Ni (1.2) [29] and SIFSIX-2-Cu-i (0.95) [31]. Comparisons of the C_2H_2 capacities and C_2H_2/CO_2 uptake ratios for the two materials and other reported materials are also exhibited in Fig. 2(b) [26–28,36–38]. Both ZU-61 and ZU-100 were located in the best performance region.

IAST selectivities were also calculated to describe the different C_2H_2/CO_2 separation abilities of the two materials, which were 5.7 and 7.6 at 1 bar (C_2H_2/CO_2 = 50/50, v/v), respectively (Fig. 2(c)). These results demonstrated that the electrostatic potential and affinity of C_2H_2 for TiF_6^{2-} were higher than those for $NbOF_5^{2-}$ due to the stronger alkalinity of TiF_6^{2-}. Then, we calculated the C_2H_2 uptakes of the two materials from C_2H_2/CO_2 (50/50, v/v) mixtures. The results seen at varying pressures are shown in Fig. 2(d) [34–36,39]. At 298 K and 1 bar, the C_2H_2 capacity of ZU-100 was the highest, 6.3 $mmol \cdot g^{-1}$, which exceeded most of the capacities reported for MOFs. The C_2H_2 capacity of ZU-61 (4.8 $mmol \cdot g^{-1}$) was slightly lower than that of ZU-100 but was still considerable. The calculated C_2H_2 capacities for C_2H_2/CO_2 (1/99, v/v) mixtures are also shown in Fig. S7 (cf. ESM). ZU-100 (0.34 $mmol \cdot g^{-1}$ at 100 kPa) and ZU-61 (0.19 $mmol \cdot g^{-1}$ at 100 kPa) still performed better than other reported MOFs.

To better understand the interactions between the adsorbent materials and guest molecules, we calculated the Q_{st} of ZU-61 and ZU-100 for C_2H_2 and CO_2 based on the adsorption isotherms collected at 283, 298 and 313 K

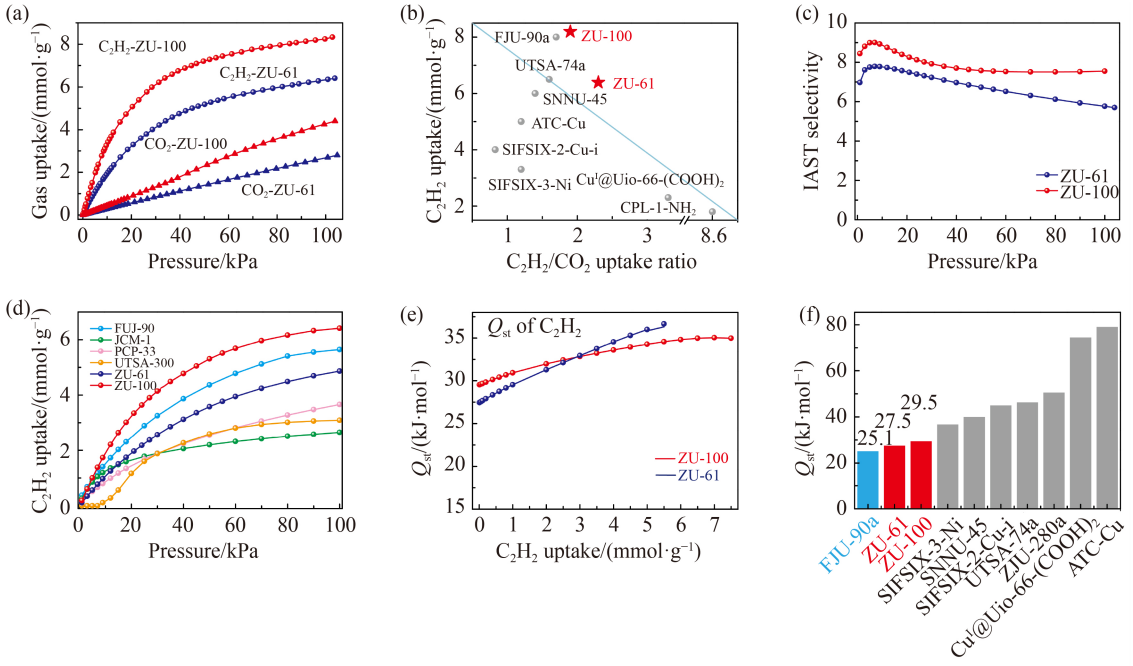

Fig. 2 (a) Single-component adsorption isotherms of C_2H_2 (red) and CO_2 (blue) on ZU-61 and ZU-100 at 298 K; (b) the comparison of C_2H_2 capacity and C_2H_2/CO_2 uptake ratio at 1 bar and 298 K with other materials; (c) ideal adsorbed solution theory (IAST) calculations of C_2H_2/CO_2 (50/50, v/v) adsorption selectivity for ZU-61 and ZU-100; (d) calculated C_2H_2 adsorption isotherms from C_2H_2/CO_2 (50/50, v/v) mixtures at 298 K [34–36,39]; (e) calculated isosteric heats of adsorption for C_2H_2 at different C_2H_2 loadings on ZU-61 and ZU-100; (f) the comparison of Q_{st} (isosteric heats of adsorption) among ZU-61, ZU-100 and other materials.

(Figs. S8–S11, cf. ESM). The curves for Q_{st} at all gas loadings are shown in Figs. 2(e) and S12 (cf. ESM). The Q_{st} values for C_2H_2 gradually increased with increasing C_2H_2 uptake, which be attributed to enhancement of guest-guest interactions. The Q_{st} values of ZU-61 and ZU-100 for C_2H_2 were 27.5 and 29.5 kJ·mol^{-1} at zero loading, respectively; these were higher than their Q_{st} values for CO_2 at zero loading (18.5 kJ·mol^{-1} for ZU-61 and 20.4 kJ·mol^{-1} for ZU-100), which indicated the stronger affinities of the two materials for C_2H_2. We noted that the Q_{st} values of C_2H_2 in ZU-61 and ZU-100 were notably lower than those of most known materials, such as SIFSIX-2-Cu-i (46.3 kJ·mol^{-1}) [31], SIFSIX-3-Ni (36.7 kJ·mol^{-1}) [29], UTSA-74a (45 kJ·mol^{-1}) [14] and SNNU-45 (40 kJ·mol^{-1}) [15], and only slightly higher than the Q_{st} of FJU-90 (25.1 kJ·mol^{-1}) [36]. The data highlighted the low generation energy requirements of ZU-61 and ZU-100 for C_2H_2, which is a crucial advantage for industrial production.

Dynamic breakthrough experiments were carried out for a C_2H_2/CO_2 (50/50, v/v) mixture at 298 K to examine the separation ability of the two materials with the C_2H_2/CO_2 mixture. As shown in Fig. 3, the breakthrough curve of ZU-61 indicated that CO_2 first eluted at 14 min·g^{-1} and then immediately approached a plateau without detectable C_2H_2, which was detected until 37 min·g^{-1} and reached a balance at 65 min·g^{-1} (Fig. 3(a)). ZU-100 showed a better performance (Fig. 3(b)). During the breakthrough test, CO_2 was first detected at 25 min·g^{-1}, while C_2H_2 was detected at 70 min·g^{-1} and reached a balance at 140 min·g^{-1}. The dynamic C_2H_2 capacities also calculated according to the breakthrough results. ZU-61 had a relatively low dynamic capacity of 1.9 mmol·g^{-1}. However, the dynamic C_2H_2 capacity of ZU-100 was stable at 4.3 mmol·g^{-1}, and this exceeded the capacities of the vast majority of MOFs, such as ZJU-280a (4.1 mmol·g^{-1}) [40], Cu^I@Uio-66-(COOH)$_2$ (2.9 mmol·g^{-1}) [28] and JCM-1 (2.2 mmol·g^{-1}) [35], which are only lower than those of SIFSIX-Cu-TPA (5.7 mmol·g^{-1}) [41] and SNNU-45 (5.2 mmol·g^{-1}) [37] (Fig. 3(c)). Breakthrough experiments under higher flows also conducted, and the dynamic C_2H_2 capacities were almost identical (Figs. S13 and S14, cf. ESM). The excellent dynamic C_2H_2 capacity of ZU-100 is vital to improving the separation efficiency, which improves the potential for industrial applications of ZU-100. Another key point for industrial application is the cycling ability. The outstanding cycling abilities of the two materials were confirmed by continuous adsorption−desorption experiments, and the results are depicted in Fig. 3(d).

To demonstrate the detailed interactions occurring between guest molecules and host frameworks, DFT method [42] was utilized (Fig. 4). The optimized adsorption binding sites of C_2H_2 and CO_2 molecules in the pores of ZU-100 are given in Figs. 4(a) and 4(b). For C_2H_2 molecules, there were altogether four C_2H_2 molecules located in one unit cell, which was consistent with the experimental result (3.7 C_2H_2 molecules per unit

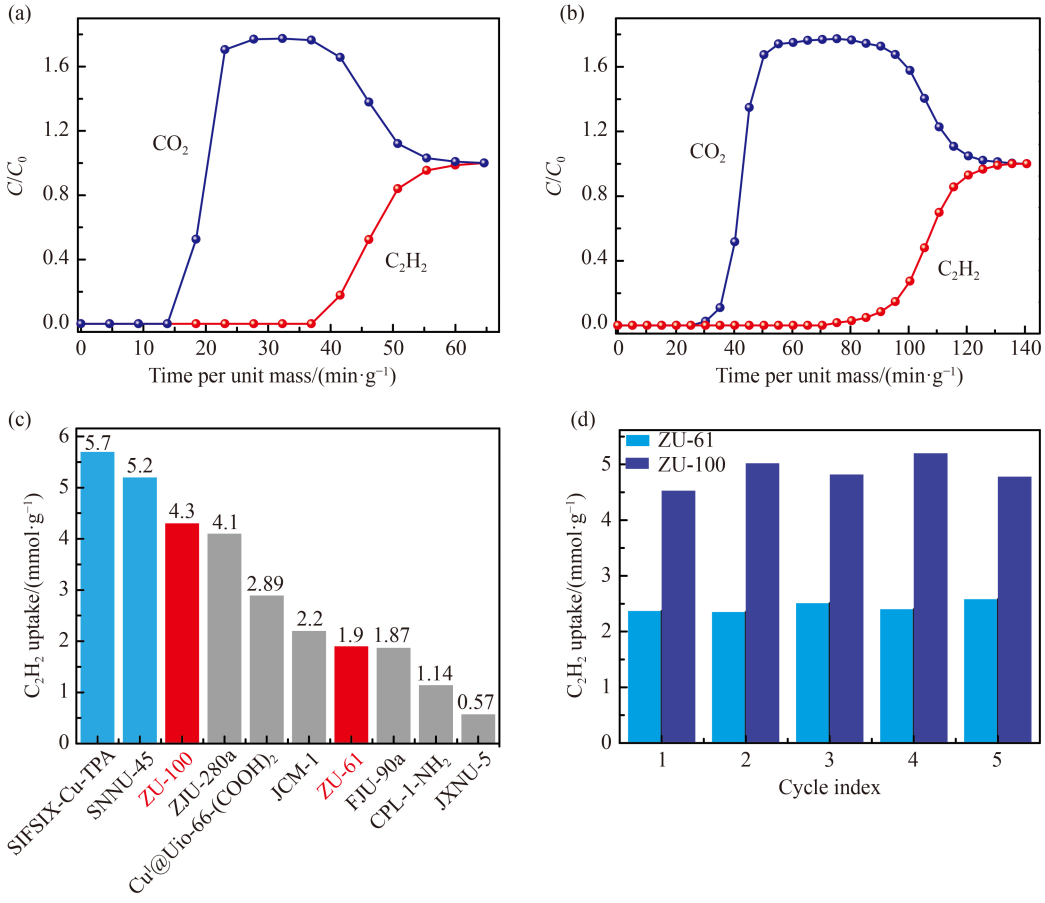

Fig. 3 Experimental dynamic breakthrough curves for C_2H_2/CO_2 (50/50, v/v) separations with (a) ZU-61 and (b) ZU-100 at 298 K and 1 bar (mixed gas flow: 2 mL·min^{-1}); (c) the comparison of dynamic C_2H_2 capacities between ZU-61, ZU-100 and some other representative MOFs; (d) cycle breakthrough tests for C_2H_2/CO_2 (50/50, v/v) separation with ZU-61 and ZU-100.

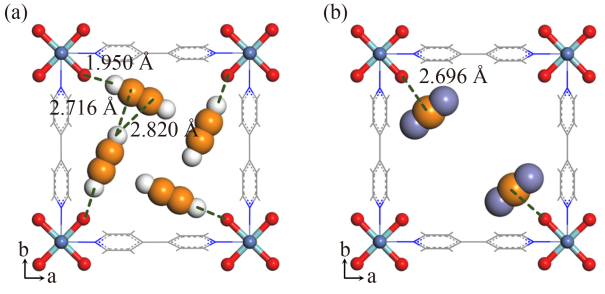

Fig. 4 Schematic pictures showing the DFT optimized (a) C_2H_2 and (b) CO_2 adsorption configurations and the distances between atoms in ZU-100 (Color code: F red; Ni and O purple; Nb and Ti cyan; N blue; C orange; H white).

cell). The strong adsorption of C_2H_2 molecules was mainly attributed to C–H···F hydrogen bonds with a distance of 1.950 Å as well as van der Waals interactions between C_2H_2 molecules and 4,4'-bipyridine linkers. Intermolecular interactions between guest C_2H_2 molecules also played an important role. The distance between neighboring adsorbed C_2H_2 molecules was ideal for them to synergistically interact with each other through formation of multiple $H^{\delta+}\cdots C^{\delta-}$ dipole–dipole interactions with distances of 2.716 and 2.820 Å. All the interactions together determined the static adsorption energy (ΔE) of C_2H_2, which was 46.9 kJ·mol^{-1}. However, CO_2 molecules only formed relatively weak van der Waals interactions with one F atom in the pores, and this exhibited a distance of 2.696 Å. Two CO_2 molecules at the diagonal positions in one unit cell were too far apart to form guest–guest interactions. The ΔE was calculated to be 28.7 kJ·mol^{-1}. DFT calculations were also conducted with ZU-61 and led to a similar conclusion, with ΔE values of 44.6 and 29.8 kJ·mol^{-1} for C_2H_2 and CO_2, respectively; these are shown in Fig. S15 (cf. ESM).

4 Conclusions

In summary, through introduction of strong adsorption sites and reasonable tuning of the pore structure and geometry, we synthesized two anion-pillared hybrid materials, ZU-100 and ZU-61, for separation of C_2H_2/CO_2 mixtures. The appropriate pores enhanced the C_2H_2 storage density (8.3 mmol·g^{-1} for ZU-100 and 6.4 mmol·g^{-1} for ZU-61 at 298 K and 1 bar) and provided sufficient

space for formation of C_2H_2 clusters, which enhanced C_2H_2 adsorption in the pores. The IAST selectivity and C_2H_2/CO_2 uptake ratio were calculated to verify the perfect C_2H_2/CO_2 separation ability. The extremely low C_2H_2 isosteric heats of adsorption (27.5 kJ·mol^{-1} for ZU-61 and 29.5 kJ·mol^{-1} for ZU-100) and the excellent dynamic breakthrough capacities for C_2H_2 (4.3 mmol·g^{-1} for ZU-100) were two highlights of ZU-100 and ZU-61 and were essential for decreasing energy consumption and improving the separation efficiencies. DFT calculations revealed the binding sites for C_2H_2 molecules in the pores, which involved both C–H···F hydrogen bonds and intermolecular interactions. CO_2 molecules formed only relatively weak van der Waals interactions with single F atoms. This work revealed the importance of appropriate adsorption sites and reasonable pore structures for hydrocarbon separation.

Acknowledgements This work was financially supported by the Zhejiang Provincial Natural Science Foundation of China (Grant No. LR20B060001), the National Natural Science Foundation of China (Grant Nos. 22122811, 21938011, and 21890764), and the Research Computing Center in College of Chemical and Biological Engineering at Zhejiang University.

Electronic Supplementary Material Supplementary material is available in the online version of this article at https://dx.doi.org/10.1007/s11705-022-2183-x and is accessible for authorized users.

References

1. Luna-Triguero A, Vicent-Luna J M, Madero-Castro R M, Gomez-Alvarez P, Calero S. Acetylene storage and separation using metal-organic frameworks with open metal sites. ACS Applied Materials & Interfaces, 2019, 11(34): 31499–31507
2. Matsuda R, Kitaura R, Kitagawa S, Kubota Y, Belosludov R V, Kobayashi T, Sakamoto H, Chiba T, Takata M, Kawazoe Y, Mita Y. Highly controlled acetylene accommodation in a metal−organic microporous material. Nature, 2005, 436(7048): 238–241
3. Xiang S, Zhou W, Gallegos J M, Liu Y, Chen B L. Exceptionally high acetylene uptake in a microporous metal−organic framework with open metal sites. Journal of the American Chemical Society, 2009, 131(34): 12415–12419
4. Foo M L, Matsuda R, Hijikata Y, Krishna R, Sato H, Horike S, Hori A, Duan J, Sato Y, Kubota Y, Takata M, Kitagawa S. An adsorbate discriminatory gate effect in a flexible porous coordination polymer for selective adsorption of CO_2 over C_2H_2. Journal of the American Chemical Society, 2016, 138(9): 3022–3030
5. Peng Y, Pham T, Li P, Wang T, Chen Y, Chen K J, Forrest K A, Space B, Cheng P, Zaworotko M J, Zhang Z. Robust ultramicroporous metal−organic frameworks with benchmark affinity for acetylene. Angewandte Chemie International Edition, 2018, 57(34): 10971–10975
6. Yao Z, Zhang Z, Liu L, Li Z, Zhou W, Zhao Y, Han Y, Chen B, Krishna R, Xiang S. Extraordinary separation of acetylene-containing mixtures with microporous metal−organic frameworks with open O donor sites and tunable robustness through control of the helical chain secondary building units. Chemistry, 2016, 22(16): 5676–5683
7. Scott H S, Shivanna M, Bajpai A, Madden D G, Chen K J, Pham T, Forrest K A, Hogan A, Space B, Perry J J IV, Zaworotko M J. Highly selective separation of C_2H_2 from CO_2 by a new dichromate-based hybrid ultramicroporous material. ACS Applied Materials & Interfaces, 2017, 9(39): 33395–33400
8. Li P, He Y, Zhao Y, Weng L, Wang H, Krishna R, Wu H, Zhou W, O'Keeffe M, Han Y, Chen B. A rod-packing microporous hydrogen-bonded organic framework for highly selective separation of C_2H_2/CO_2 at room temperature. Angewandte Chemie International Edition, 2015, 54(2): 574–577
9. Zhang L, Jiang K, Zhang J, Pei J, Shao K, Cui Y, Yang Y, Li B, Chen B, Qian G. Low-cost and high-performance microporous metal−organic framework for separation of acetylene from carbon dioxide. ACS Sustainable Chemistry & Engineering, 2019, 7(1): 1667–1672
10. Zhang J, Chen X. Optimized acetylene/carbon dioxide sorption in a dynamic porous crystal. Journal of the American Chemical Society, 2009, 131(15): 5516–5521
11. Qazvini O, Babarao R, Telfer S. Multipurpose metal-organic framework for the adsorption of acetylene: ethylene purification and carbon dioxide removal. Chemistry of Materials, 2019, 31(13): 4919–4926
12. Moreau F, da Silva I, Al Smail N, Easun T, Savage M, Godfrey M, Parker S, Manuel P, Yang S, Schroder M. Unravelling exceptional acetylene and carbon dioxide adsorption within a tetra-amide functionalized metal−organic framework. Nature Communications, 2017, 8(1): 14085
13. Zhang Y, Hu J, Krishna R, Wang L, Yang L, Cui X, Duttwyler S, Xing H. Rational design of microporous MOFs with anionic boron cluster functionality and cooperative dihydrogen binding sites for highly selective capture of acetylene. Angewandte Chemie International Edition, 2020, 59(40): 17664–17669
14. Liu R, Liu Q, Krishna R, Wang W, He C, Wang Y. Water-stable europium 1,3,6,8-tetrakis(4-carboxylphenyl)pyrene framework for efficient C_2H_2/CO_2 separation. Inorganic Chemistry, 2019, 58(8): 5089–5095
15. Xie Y, Cui H, Wu H, Lin R, Zhou W, Chen B. Electrostatically driven selective adsorption of carbon dioxide over acetylene in an ultramicroporous material. Angewandte Chemie International Edition, 2021, 60(17): 9604–9609
16. Wang J, Zhang Y, Su Y, Liu X, Zhang P, Lin R, Chen S, Deng Q, Zeng Z, Deng S, Chen B. Fine pore engineering in a series of isoreticular metal−organic frameworks for efficient C_2H_2/CO_2 separation. Nature Communications, 2022, 13(1): 200
17. Qazvini O, Babarao R, Telfer S. Selective capture of carbon dioxide from hydrocarbons using a metal−organic framework. Nature Communications, 2021, 12(1): 197
18. Choi D, Kim D, Kang D, Kang M, Chae Y, Hong C. Highly selective CO_2 separation from a CO_2/C_2H_2 mixture using a diamine-appended metal−organic framework. Angewandte Chemie International Edition, 2021, 9(37): 21424–21428

19. Shi Y, Xie Y, Cui H, Ye Y, Wu H, Zhou W, Arman H, Lin R, Chen B. Highly selective adsorption of carbon dioxide over acetylene in an ultramicroporous metal−organic framework. Advanced Materials, 2021, 33(45): 2105880
20. Ye Y, Xian S, Cui H, Tan K, Gong L, Liang B, Pham T, Pandey H, Krishna R, Lan P, Forrest K A, Space B, Thonhauser T, Li J, Ma S. Metal−organic framework based hydrogen-bonding nanotrap for efficient acetylene storage and separation. Journal of the American Chemical Society, 2022, 144(4): 1681–1689
21. Dong Q, Zhang X, Liu S, Lin R, Guo Y, Ma Y, Yonezu A, Krishna R, Liu G, Duan J, Matsuda R, Jin W, Chen B. Tuning gate-opening of a flexible metal−organic framework for ternary gas sieving separation. Angewandte Chemie International Edition, 2020, 59(50): 22756–22762
22. Fan W, Yuan S, Wang W, Feng L, Liu X, Zhang X, Wang X, Kang Z, Dai F, Yuan D, Sun D, Zhou H C. Optimizing multivariate metal−organic frameworks for efficient C_2H_2/CO_2 separation. Journal of the American Chemical Society, 2020, 142(19): 8728–8737
23. Pei J, Shao K, Wang J, Wen H, Yang Y, Cui Y, Krishna R, Li B, Qian G. A chemically stable hofmann-type metal−organic framework with sandwich-like binding sites for benchmark acetylene capture. Advanced Materials, 2020, 32(24): 1908275
24. Mukherjee S, He Y, Franz D, Wang S, Xian W, Bezrukov A, Space B, Xu Z, He J, Zaworotko M. Halogen-C_2H_2 binding in ultramicroporous metal−organic frameworks (MOFs) for benchmark C_2H_2/CO_2 separation selectivity. Chemistry, 2020, 26(22): 4923–4929
25. Kumar N, Mukherjee S, Harvey-Reid N, Bezrukov A, Tan K, Martins V, Vandichel M, Pham T, van Wyk L, Oyekan K, Kumar A, Forrest K A, Patil K M, Barbour L J, Space B, Huang Y, Kruger P E, Zaworotko M J. Breaking the trade-off between selectivity and adsorption capacity for gas separation. Chem, 2021, 7(11): 3085–3098
26. Yang L, Yan L, Wang Y, Liu Z, He J, Fu Q, Liu D, Gu X, Dai P, Li L, Zhao X. Adsorption site selective occupation strategy within a metal−organic framework for highly efficient sieving acetylene from carbon dioxide. Angewandte Chemie International Edition, 2021, 60(9): 4570–4574
27. Luo F, Yan C, Dang L, Krishna R, Zhou W, Wu H, Dong X, Han Y, Hu T L, O'Keeffe M, Wang L, Luo M, Lin R B, Chen B. UTSA-74: a MOF-74 isomer with two accessible binding sites per metal center for highly selective gas separation. Journal of the American Chemical Society, 2016, 138(17): 5678–5684
28. Zhang L, Jiang K, Yang L, Li L, Hu E, Yang L, Shao K, Xing H, Cui Y, Yang Y, Li B, Chen B, Qian G. Benchmark C_2H_2/CO_2 separation in an ultra-microporous metal−organic framework via copper(I)-alkynyl chemistry. Angewandte Chemie International Edition, 2021, 60(29): 15995–16002
29. Chen K J, Scott H, Madden D, Pham T, Kumar A, Bajpai A, Lusi M, Forrest K, Space B, Perry J IV, Zaworotko M J. Benchmark C_2H_2/CO_2 and CO_2/C_2H_2 separation by two closely related hybrid ultramicroporous materials. Chem, 2016, 1(5): 753–765
30. Jiang M D, Cui X L, Yang L F, Yang Q W, Zhang Z Q, Yang Y W, Xing H B. A thermostable anion-pillared metal−organic framework for C_2H_2/C_2H_4 and C_2H_2/CO_2 separations. Chemical Engineering Journal, 2018, 352: 803–810
31. Cui X, Chen K, Xing H, Yang Q, Krishna R, Bao Z, Wu H, Zhou W, Dong X, Han Y, Li B, Ren Q, Zaworotko M J, Chen B. Pore chemistry and size control in hybrid porous materials for acetylene capture from ethylene. Science, 2016, 353(6295): 141–144
32. Nugent P, Belmabkhout Y, Burd S, Cairns A, Luebke R, Forrest K, Pham T, Ma S, Space B, Wojtas L, Eddaoudi M, Zaworotko M J. Porous materials with optimal adsorption thermodynamics and kinetics for CO_2 separation. Nature, 2013, 495(7439): 80–84
33. Cui X, Niu Z, Shan C, Yang L, Hu J, Wang Q, Lan P C, Li Y, Wojtas L, Ma S, Xing H. Efficient separation of xylene isomers by a guest-responsive metal−organic framework with rotational anionic sites. Nature Communications, 2020, 11(1): 5456
34. Lin R B, Li L, Wu H, Arman H, Li B, Lin R G, Zhou W, Chen B. Optimized separation of acetylene from carbon dioxide and ethylene in a microporous material. Journal of the American Chemical Society, 2017, 139(23): 8022–8028
35. Lee J, Chuah C Y, Kim J, Kim Y, Ko N, Seo Y, Kim K, Bae T H, Lee E. Separation of acetylene from carbon dioxide and ethylene by a water-stable microporous metal−organic framework with aligned imidazolium groups inside the channels. Angewandte Chemie International Edition, 2018, 57(26): 7869–7873
36. Ye Y, Ma Z, Lin R B, Krishna R, Zhou W, Lin Q, Zhang Z, Xiang S, Chen B. Pore space partition within a metal−organic framework for highly efficient C_2H_2/CO_2 separation. Journal of the American Chemical Society, 2019, 141(9): 4130–4136
37. Li Y, Wang Y, Xue Y, Li H, Zhai Q, Li S, Jiang Y, Hu M, Bu X. Ultramicroporous building units as a path to bi-microporous metal−organic frameworks with high acetylene storage and separation performance. Angewandte Chemie International Edition, 2019, 58(38): 13590–13595
38. Niu Z, Cui X, Pham T, Verma G, Lan P, Shan C, Xing H, Forrest K, Suepaul S, Space B, Nafady A, Al-Enizi A M, Ma S. A MOF-based ultra-strong acetylene nano-trap for highly efficient C_2H_2/CO_2 separation. Angewandte Chemie International Edition, 2021, 60(10): 5283–5288
39. Duan J, Jin W, Krishna R. Natural gas purification using a porous coordination polymer with water and chemical stability. Inorganic Chemistry, 2015, 54(9): 4279–4284
40. Qian Q, Gu X, Pei J, Wen H, Wu H, Zhou W, Li B, Qian G. A novel anion-pillared metal−organic framework for highly efficient separation of acetylene from ethylene and carbon dioxide. Journal of Materials Chemistry A, 2021, 9(14): 9248–9255
41. Li H, Liu C, Chen C, Di Z, Yuan D, Pang J, Wei W, Wu M, Hong M. An unprecedented pillar-cage fluorinated hybrid porous framework with highly efficient acetylene storage and separation. Angewandte Chemie International Edition, 2021, 60(14): 7547–7552
42. Zhang Z, Cui X, Jiang X, Ding Q, Cui J, Zhang Y, Belmabkhout Y, Adil K, Eddaoudi M, Xing H. Efficient splitting of trans-/cis-olefins using an anion-pillared ultramicroporous metal−organic framework with guest-adaptive pore channels. Engineering, 2022, 11: 80–86